Kinetik: Game Technology, Information System, Computer Network, Computing, Electronics, and Control
Journal homepage: http://kinetik.umm.ac.id
ISSN: 2503-2267
Vol. 8, No. 3, August, Pp. 663-672

Designing a smart inverter for voltage sag compensation due to motor start-up

Indra Budi Hermawan[1,2], Mochamad Ashari[1*], Dedet Candra Riawan[1]
Department of Electrical Engineering, Institut Teknologi Sepuluh Nopember, Surabaya, Indonesia[1]
Department of Electrical Technology, Faculty of Vocations, Universitas 17 Agustus 1945, Surabaya, Indonesia[2]

Article Info
Keywords:
Voltage Sag Recovery, Smart Inverter, Artificial Intelligent Controller, Inrush Current Induction Motor, Power Quality Improvement, PV Farm ancillary function

Article history:
Received: May 31, 2023
Accepted: July 01, 2023
Published: August 31, 2023

Cite:
I. Budi Hermawan, A. Mochamad, and D. Candra Riawan, "Designing a Smart Inverter for Voltage Sag Compensation Due to Motor Start-up", KINETIK, vol. 8, no. 3, Aug. 2023. https://doi.org/10.22219/kinetik.v8i3.1744

*Corresponding author.
Mochamad Ashari
E-mail address:
ashari@ee.its.ac.id

Abstract
Starting a large induction motor will always follow up with an inrush current as the nature of an induction motor. On a less stiff power system, that inrush current will be causing a Voltage Sag (VS). A big VS can lead to significant disruptions in power quality and reliability. To address this, a Smart Inverter with an Artificial Intelligence (AI) -driven controller installed in a Photovoltaic (PV) farm is proposed for voltage sag recovery. During normal conditions, the PV farm acts as a power source supporting the main grid, but when large induction motors are started, the smart inverter connected to the PV is responsible for power conversion to recover sags caused by the Induction motor inrush current. The controller inside the Inverter ensures optimal operation. The use of AI also compares the effectiveness of using the Fuzzy Logic Controller (FLC) with the Proportional Integral (PI) Controller to assess their performance in reducing current spikes. Based on simulations, the FLC outperformed PI Controller in mitigating the voltage sag and avoiding the Low Voltage Ride-Through (LVRT). Simulation results show that voltage sag can be recovered for up to 97% of the nominal voltage, a significant improvement over the 80% sag recovery without the smart Inverter. At a nominal grid voltage of 6,600 volts, the VS Magnitude was successfully increased from 5,210 volts to 6,368 volts and the VS Duration also decreased from 6.96 s to 4.97 s. The results achieved validate the effectiveness of the approach in improving the power quality.

1. Introduction

Besides its advantages, the classical issue with an Induction motor is the large inrush current following the motor starting. For a less stiff power source, the direct effect of the large inrush current is a Voltage sag (VS). With inrush currents, the high current drawn by a large induction motor starting up leads to a deep VS. A VS is maintained at a magnitude and duration greater than the allowable limit [1], [2]. Figure 1 shows the voltage limit curve during sags. It exceeds the Low Voltage Ride Through (LVRT) of the generator curve. When the voltage drops below the LVRT curve, blackouts may occur. The LVRT curve is used as the fundamental reference for configuring relay protection, especially in mini-grid or isolated systems. LVRT is defined as the generator's ability to tolerate voltage drops and remain connected to the power grid [3]. In the event of a disturbance in the electrical system, the network may experience a temporary voltage decrease, which the protection relay reads as a disturbance. Suppose the magnitude and duration of the VS are greater than the generator's Under Voltage relay protection is configured for, the generator or distribution system will disconnect from the network. To prevent this, the VS must not drop below the LVRT curve so the connection of the generator with the grid is maintained [4].

In many countries, the LVRT curve adapts to the conditions of the electrical system, such as with NERC, Polygonal, and FERC, which are implemented in North American countries and Canada [5]. In Indonesia, regulations regarding LVRT are stipulated by the Regulation of the Minister of Energy and Mineral Resources of the Republic of Indonesia of 2020, concerning Regulations for Electric Power System Networks (Grid Code) [6]. Chapter 4.4.3.3 states that all generating units must be able to operate at low (LVRT) and high voltages (HVRT). According to the LVRT curve shown in Figure 1, the grid's voltage drops to below 80 – 85 % of the nominal voltage at t = 2 – 15 seconds can cause the generator to disconnect from the grid.

Numerous studies have attempted to identify a safe and effective method for starting a large medium-voltage induction motor without compromising the voltage level of the network, like autotransformers, for example [7]. Static Compensator (STATCOM), Dynamic Voltage Restorer (DVR), and Unitary Power Quality Conditioner (UPQC) are detailed devices used to solve this problem [8].

To mitigate VSs, an external energy source is needed. With increasingly limited access to conventional energy sources, various renewable energy sources are being scrutinized to find the best source for renewable energy, such as wind turbines [9], [10], wave energy, and geothermal energy [11].

Research into PV systems as a renewable energy source to mitigate LVRT exists [12 - 16]. Another PV-related LVRT study demonstrated the use of a data extraction technique on the power grid to obtain accurate transient data [15]. This research studies the potential of PV in LVRT mitigation with a focus on inverter control methods [12], [13] and also discusses LVRT mitigation in relatively weak power grids [14].

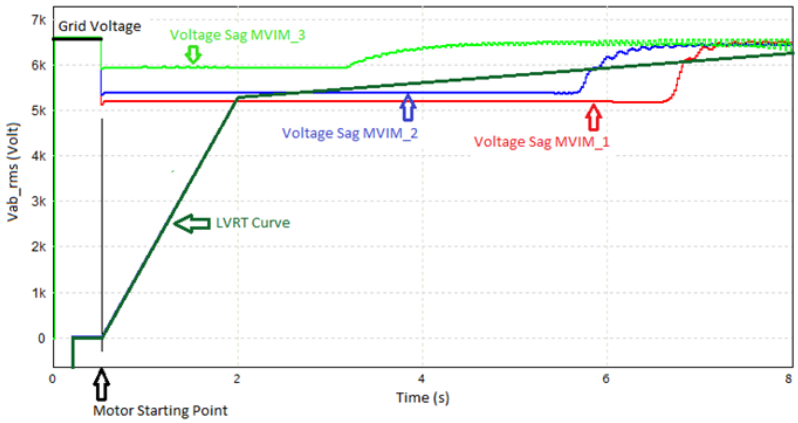

Figure 1. Voltage sags (MVIM 1-3) and the minimum voltage before blackout occurs

The energy required for VS mitigation is substantial and is obtained from renewable energy sources and needs to be stored and ready for immediate use. The ideal energy storage for this purpose is a supercapacitor (SC). The use of an SC as an energy storage medium to mitigate fluctuations in voltage and electric power was studied by [17-19]. The use of an SC on a Medium Voltage Grid has also become something of interest for more detailed research [20].

An inverter is the main component to distribute power from energy storage media to the grid. The inverter converts the Direct Current (DC) into an Alternating Current (AC) that corresponds to the AC voltage of the power grid. Many researches have been conducted on inverter topology and design. Researches on inverters related to VS and solutions to LVRT problems include [21], [22]. Guanyu et. al emphasized using a Phase-Locked Loop to synchronize the inverter connected to the grid in case of a VS or LVRT. Meanwhile, a PV grid-tied generator capable of overcoming VS through a control strategy on an inverter that will inject reactive power into the grid in the event of a voltage drop is also proposed [22], [23].

This paper offers research that uses motor data used in factories, and is simulated to be able to overcome Voltage Sags that occur. From the several previous research papers that have been described, in this study improvements were made by adding artificial intelligence to improve the performance of the inrush current compensator. The main result achieved was a significant improvement in terms of reducing the magnitude and duration of the Voltage Sag.

The paper is organized with the dynamic model of the system presented in Section 2. The test system and AI method for the inverter are described in Section 3. The simulation results are presented and discussed in Section 4. Finally, the conclusions and contributions to this paper are presented in Section 5.

2. Dynamic Model of the Electrical System

2.1 Plant Single-line Diagram

In this study, three induction motors were simulated within the electrical system with a 4500 hp Medium Voltage Induction Motor-1 (MVIM-1), 2250 hp Medium Voltage Induction Motor-2 (MVIM-2), and 600 hp Medium Voltage Induction Motor-3 (MVIM-3). These motors received their electricity supply from a 6.6 kV bus connected to a 20/6.6 kV 8 MVA step-down Power Transformer (PT). The primary side of the transformer was connected to the 20 kV electrical grid at a main substation. The secondary side was the 6.6 kV bus which supplied the induction motors and the low Voltage Transformer (VT).

The production process at this plant required a specific starting sequence for existing induction motors. The operational sequence started at MVIM-1, followed by MVIM-2, and finally MVIM-3. A common obstacle is the voltage level on the 6.6 kV bus, which is still unrecovered when the next induction motor is started. It often affects power quality and stability and can cause the electrical system to go out. The duration of the VS caused by MVIM-1 starting is ~6 seconds, as has been simulated. In the uncompensated condition, the VS causes the grid voltage to drop below the LVRT curve line. Preventing the voltage drop requires intervention so that the voltage at the 6.6 kV bus can return to its normal level as soon as the next induction motor starts.

2.2 PV Compensation Method for Inrush Current of MVIM

Energy obtained from sunlight (photovoltaic energy) has great potential if successfully used to improve the power quality and stability of a power system network. In this study, power quality was improved by injecting electrical energy obtained from PV to supply electrical energy and also by injecting an electric current to help overcome inrush currents when starting an induction motor. The energy required to overcome the inrush current is quite large, so the energy from the PV needs to be collected and stored in an SC to be used on demand.

The energy was then converted into AC voltage, as required to meet the plant's electrical requirements. The single-line diagram in Figure 2 shows that energy entering the plant originates from the grid and the inverter. By using Kirchhoff's first law, the equation for the electric current entering the MVIM can be obtained. The Equation is shown in Equation 1.

$$I_{MVIM} = I_{Grid} + I_{INV} \tag{1}$$

where: I_{MVIM} is the induction motor current, I_{Grid} is the grid current, and I_{INV} is the inverter current that is injected into the system.

The inverter utilized was a VSI that converts the DC voltage from the SC to AC voltage based on the grid's voltage. The VT and Current Transformer (CT) provided the input signal to the Pulse Width Modulation (PWM) circuit The PWM circuit works based on an AI algorithm and uses these two input signals to adjust the frequency, phase angle, and other AC voltage parameters to produce a trigger signal. This trigger signal is used to drive the power electronics circuit on the VSI. The output of the VSI is an alternating current signal that is in phase with the alternating current on the grid. The inverter output voltage level need to be stepped up to the grid voltage level. Therefore, a PT is required to increase the inverter voltage to meet the grid voltage level

When the plant is running normally without the induction motor starting, the PV inverter functions to bear part of the plant's electrical load. When the induction motor is being started, the PV inverter helps to offset some of the inrush currents that arise. The magnitude of the PV inverter current varies according to the control method used. In this study, three types of current injection methods were used to find which best mitigated the VS. They were fixed compensation, PI controller, and FLC. The equations for the INV currents are Equation 2, Equation 3, and Equation 4. I_{INV_fixed} is the current resulting from the fixed compensation, I_{INV_PI} is the current resulting from the PI controller, and $I_{INV\text{-}FLC}$ is the current resulting from the FLC.

$$I_{INV\_fixed} = EN\ x\ 0.8\ I_{MVIM} \tag{2}$$

$$I_{INV\_PI} = EN\ x\ PI_{constant} \tag{3}$$

$$I_{INV\_FLC} = EN\ x\ FLC_{constant} \tag{4}$$

where the constants $PI_{constant}$ and $FLC_{constant}$ refer to the results of the PI controller and FLC calculations.

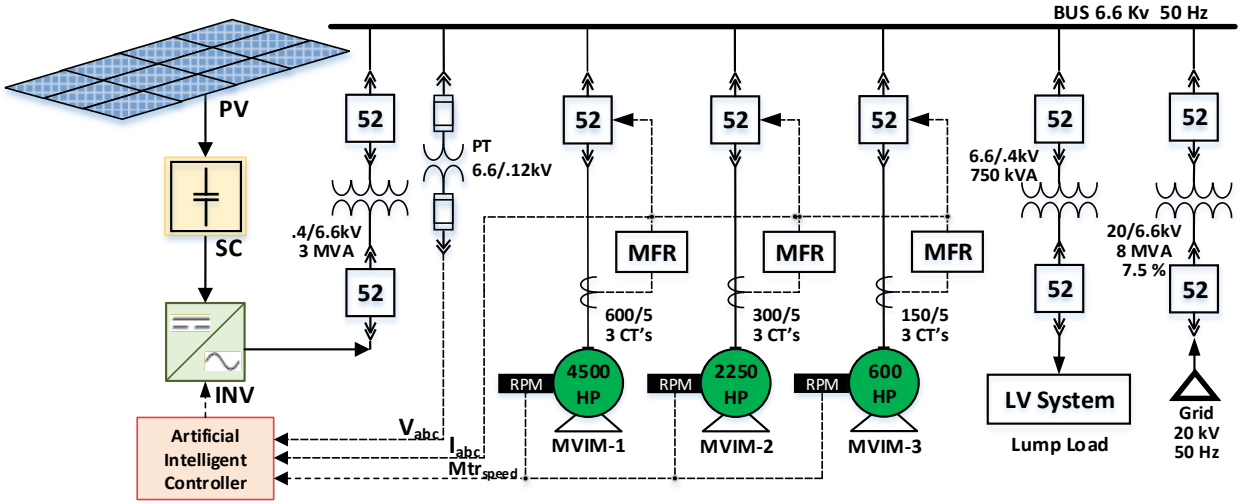

Figure 2. Single-line diagram of the electrical system studied

3. Controlled Voltage Sag Mitigation

3.1 Fixed Compensation

Previous research [25] showed that compensation of 80% of the inrush current can reduce the magnitude of the VS so that the grid voltage can be maintained above the safe limit as stipulated in the regulations regarding LVRT listed in the regulation of the Minister of Energy and Mineral Resources of the Republic of Indonesia of 2020 concerning Regulations for Electric Power System Networks (Grid Code) [6]. However, this method requires revision, as when the voltage drop reaches a safe level, the constant compensation during an Inrush current causes energy to be wasted. The result is that the energy reserves of the SC rapidly decrease.

3.2 PID Control Compensation

Conventional Proportional Integral and Derivative (PID) controllers have advantages, such as their simple program structure, high resistance to interference, wide use of controller designs in various fields, and ease of being simulated in a system. However, they require accurate parameter adjustments to get the desired results. Changes to the system parameters require adjustments to the control parameters. In this study, the PID method is used as a controller to calculate the compensation when an inrush current occurs on the grid. The PID parameters were obtained from optimization theories and validated with experiments. This way, optimal compensation results can be obtained. An ideal basic PID equation is shown in Figure 3. The PI control equation base on Figure 3 is (5) [26].

$$M = K_c \left[E + \frac{1}{T_i} \int E.dt + T_d \frac{dE}{dt} \right] + C \tag{5}$$

The algorithm in Equation 5 is an analog time domain version. Equation 6 shows it in a simpler form.

$$u(s) = K_p\, e(s) + K_i\, e(s) + K_d\, s\, e(s) \tag{6}$$

where K_p is the proportional gain, K_i is the integral gain, K_d is the derivative gain, e is the error and u(s) is the control signal.

The PID controller in this study did not use differential control because it would make the system unstable. It only used proportional and integral controls. The PI controller block diagram used in this paper is shown in Figure 4.

3.3 Fuzzy Logic Control Compensation

An adaptive controller is needed to compensate for the PI controller's inability to anticipate rapid inrush current changes or fluctuations. In this study, the Fuzzy Logic Controller (FLC) was used to improve the mitigation performance displayed by the PI controller. The advantage of FLC over PI controllers is that it allows the inclusion of several digits of human deductive reasoning in the control system. This provides the advantage of reducing dependence on mathematical models. Another advantage is that changes in the magnitude of the inrush current can be anticipated accurately.

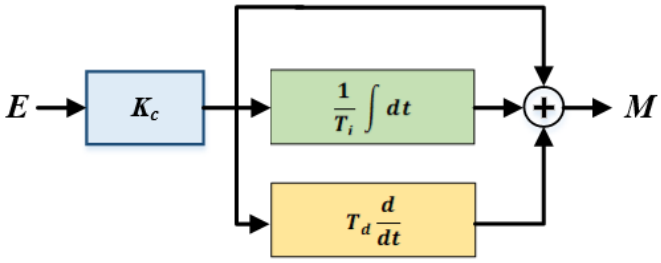

Figure 3. Diagram of the ideal PID controller

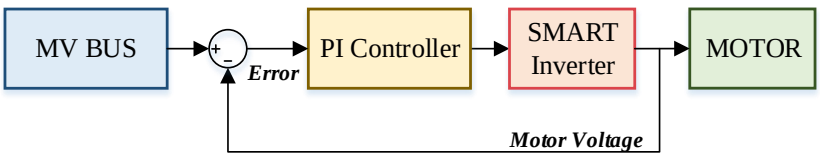

Figure 4. Proposed PI controller scheme

The FLC structure generally consists of four main parts, namely: fuzzification, rule base, inference system, and defuzzification. Fuzzification is a system input interface that uses fuzzy linguistic variables and membership functions to convert real data (crisp) into fuzzy sets. The rule base is a set of fuzzy IF-THEN rules which include premises and implications. These rules define controller behavior based on input conditions. The fuzzy inference system relates to the decision-making process for applying the rule base. Defuzzification converts fuzzy inference results into outputs that can be expressed in crisp logic. In other words, defuzzification is the reverse process of fuzzification by converting Fuzzy sets into data. This study uses the Mamdani Fuzzy type, or what is often called the min-max method, for its relatively simple application [25].

The FLC controls the compensation value (%) to be injected into the system. The greater the VS, the greater the current compensation value. The FLC inputs are the magnitude of the VS and the change in delta voltage sag (DVS). The VS value is obtained from the deviation of the 6.6 kV nominal grid voltage. The FLC output is a control signal for the inverter to determine how much compensation current is to be injected into the system.

VS and DVS as FLC input variables are transformed into input membership functions, as shown in Figure 6 and Figure 7. The VS input membership function is divided into four linguistic labels, namely: Save, Small, Big, and Very Big. The DVS input membership function is also divided into four linguistic labels, namely: D-Save, D-Small, D-Big, and D-VeryBig.

The FLC output is a control signal which determines the inrush current compensation. The FLC output membership function is shown in Figure 8. The FLC output function is divided into five linguistic labels, namely: Low, Medium, High, and Very High. The logical rules built into the inference mechanism are based on observations embodied through language variables and are rule-based. The FLC rules in the proposed method use 16 rule bases, which are represented in a symmetrical form, as shown in Figure 5.

To make it easier to interpret the FLC's percentage of compensation, a Fuzzy Surface was used, as shown by the surface curve in Figure 9. It consists of 3 axes, namely SAG, DeltaSag, and Compensation. The horizontal axis is the input and the vertical axis is the output curve. The results of the FLC calculation for determining the compensation based on the input received are clear.

Delta-Voltage Sag (DVS)	Voltage Sag (VS)			
	Save	Small	Big	Very Big
D-Save	Low	Medium	Very High	Very High
D-Small	Medium	Medium	Very High	Very High
D-Big	Medium	Medium	Very High	Very High
D-Very Big	Medium	High	Very High	Very High

Figure 5. Fuzzy rule-based for VS compensation

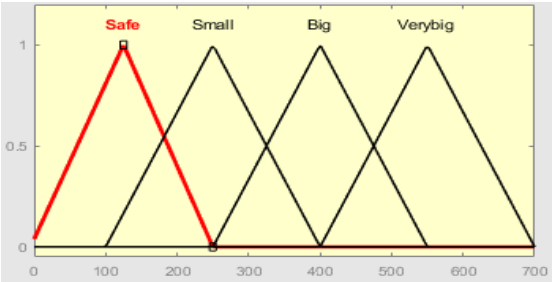

Figure 6. Voltage sag input fuzzy MF

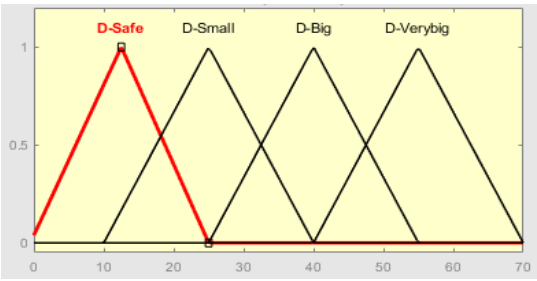

Figure 7. Delta voltage sag input fuzzy MF

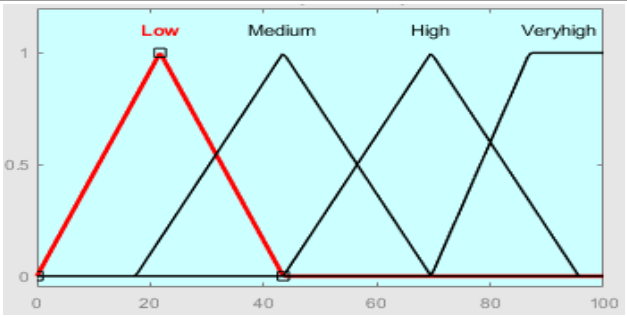

Figure 8. Voltage sag compensation output fuzzy MF

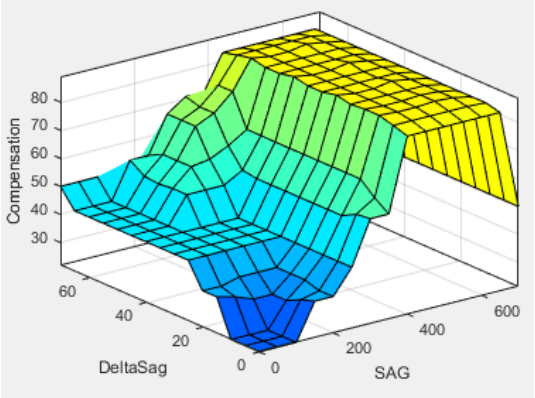

Figure 9. Fuzzy surface for voltage sag compensation

4. Results and Discussion

4.1 Motor and Grid Compensations Parameters

The MVIM-1 used in this system had four poles and a stator speed of 1500 rpm. The datasheet shows that the rotor speed reached 1491 rpm after 6 seconds. Figure 10 shows four curves, which describe the motor speed curve without compensation (Mtr1_SpeedL), the motor speed curve with constant compensation (Mtr1_speed), the motor speed curve using the PID controller (Mtr1_speedP), and the motor speed curve using the FLC (Mtr1_speedF). Figure 9 shows the difference between the compensation curve and the uncompensated curve. Without compensation, motors connected to a weak grid take longer to reach their rated speed. By compensating, the nominal speed of the motor can be reached sooner.

Compensating with an FLC allowed for the motor's nominal speed to be reached in the shortest amount of time, followed by the PID controller with fixed compensation. The motor speed curve in Figure 10 shows that the nominal speed of the motor is reached at the latest by the motor starting without compensation.

The compensation current curves from the compensation methods are shown in Figure 11. The magnitude of the compensation current looks almost identical. The difference is in the current injection time. The compensation curve using the FL (Ica-rmsF) method had the shortest time on the compensation flow curve. Compensation with the fixed compensation method (Ica_rms) had the longest injection time. The current compensation time depends on when the nominal speed of the induction motor that is being started is reached. Based on the initial formula, the compensation current was determined from the nominal speed of the induction motor that is being started.

In this study, the nominal speed of the induction motor was used as the enable (EN) signal in Equation 2, Euqation 3, and Equation 4, and the electric current injection was channeled into the 6.6 kV bus as an additional current when the motor had not reached its nominal speed. When the nominal speed of the motor was reached, the EN signal would be zero and the electric current injection from the inverter would stop. The Ica_rmsL curve in Figure 11 shows the curve starting at zero, indicating that there was no compensation current injected into the system.

Figure 12 shows the voltage drop that occurred at the 6.6 kV bus when the MVIM-1 was being started. Four curves are depicted, which reference the different compensation methods. The compensation current in the figure is enlarged so that the difference in magnitude and duration of compensation that occurred can be seen more clearly. The Vab_rms_66L curve shows the biggest drop in voltage, resulting from a large inrush current without PV compensation. The voltage drop on the other three curves was not significant. The differences were, however, in the voltage recovery times. Vab_rms_66F shows the effect of FL compensation, which seems to have normalized the fastest. The second fastest voltage drop recovery came from the PI control method (Vab_rms_66P), followed by the fixed compensation method (Vab_rms_66L).

The energy used to compensate for the inrush current is stored in an SC. If the voltage on the SC drops below 756 volts, there will be under-modulation in the inverter [25]. The SC voltage must therefore be maintained so that the SC voltage it does not fall below 756 volts.

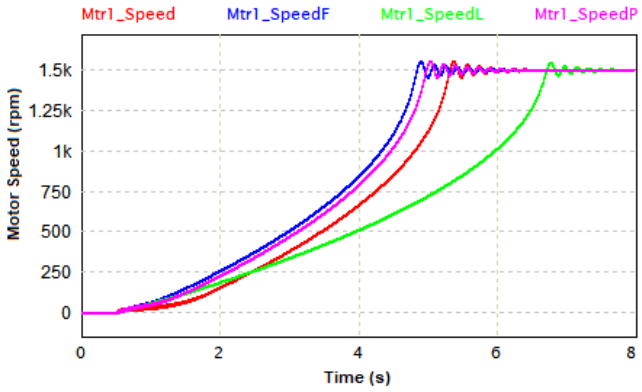

Figure 10. Motor speed comparison

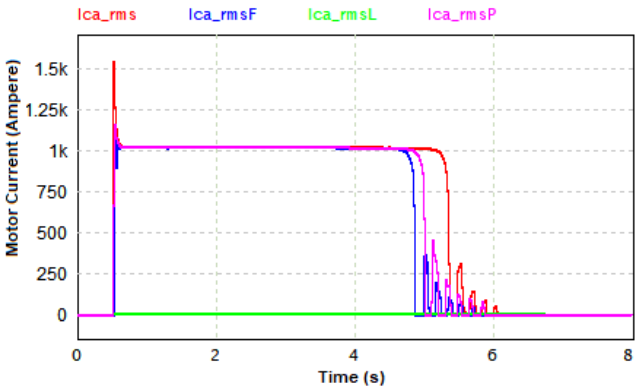

Figure 11. Current compensation

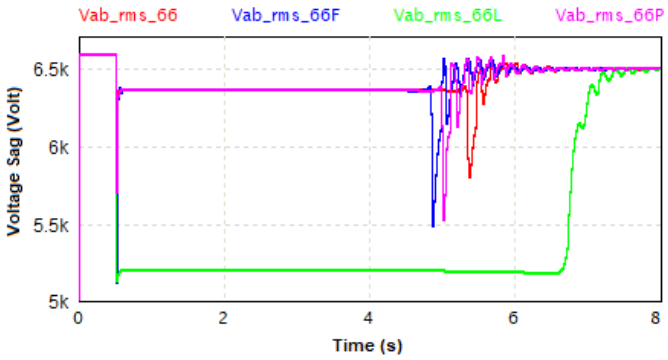

Figure 12. Voltage sag on the grid after compensation

4.2 VS Recovery and LVRT Mitigation

Figure 13 shows the voltages on the grid during a VS caused by an inrush current of MVIM-1. The graph in Figure 13 shows a decrease in the grid voltage level, comparing the MVIM-1 starting with and without compensation. PV compensation helped the grid voltage remain above 85% of the nominal grid voltage at the time of starting MVIM-1. Without PV compensation, the voltage dropped below 80%.

The results obtained from the implementation of a smart inverter to mitigate the voltage sag induced by the inrush current of an induction motor were highly successful. Prior to the intervention, the voltage sag during inrush current events fell below the critical threshold of as specified by the Indonesian government's power quality regulation, known as the Low-Voltage Ride-through (LVRT) curve. However, with the integration of the smart inverter, the voltage sag was

effectively recovered, surpassing the targeted threshold outlined in the LVRT curve. This outcome signifies a remarkable improvement in power quality, ensuring that the voltage remains within acceptable limits during inrush current events. The smart inverter's advanced control algorithms and sensing capabilities played a pivotal role in swiftly detecting and compensating for voltage sags, enabling the induction motor system to operate reliably and maintain uninterrupted performance. These findings demonstrate the potential of smart inverters as a reliable solution for minimizing voltage sag issues caused by the inrush current of induction motors while adhering to government regulations and ensuring optimal power quality.

This study's final results (Figure. 13) demonstrate the successful reduction of electrical power consumption through the integration of the PV farm, as well as its ability to alleviate the strain caused by inrush current during induction motor startup. In the first 5 seconds, the PV farm's contribution of 25% of the plant's electrical power demand during regular operation, significantly reduced reliance on the conventional power grid, resulting in improved energy efficiency and cost-effectiveness. Moreover, the SC system within the inverter effectively supplied approximately 85% of the inrush current requirement, providing a power consumption reduction from 19 to 12 MVA throughout the 5 seconds of MVIM-1 startup.

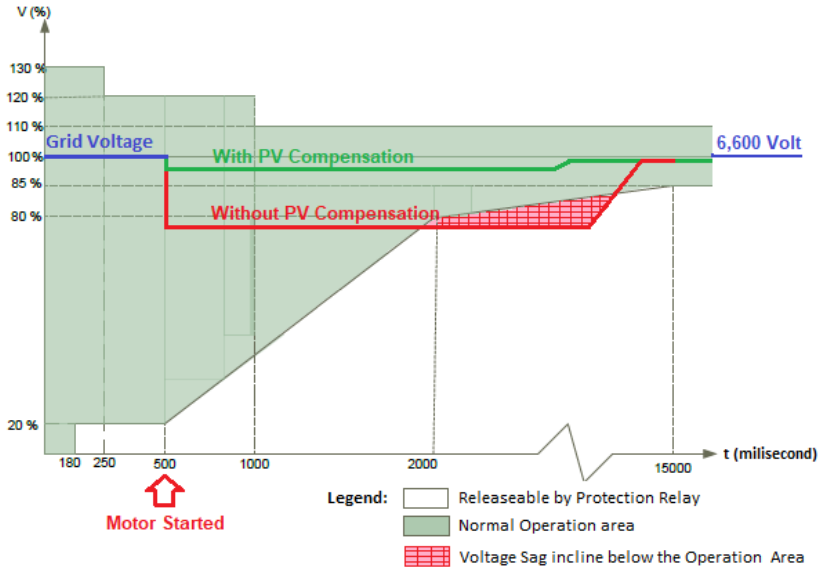

Figure 12. LVRT mitigation

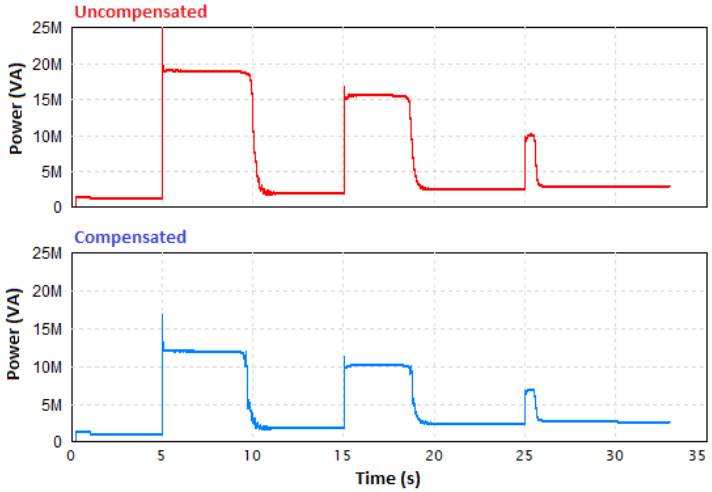

Figure 13. Grid power during MVIM motor starting with and without PV compensation

5. Conclusion

This study investigated the effectiveness of a PV farm in compensating for a decrease in grid voltage caused by inrush current. The energy the PV farm obtains is stored in an SC and converted to AC voltage using a VSI to amplify the electric current, which is absorbed in large quantities when an induction motor is started. The electric currents

injected into the system are controlled using several methods. Previous research using fixed compensation when this research is improving the compensation by utilizing the Artificial Intelligent controller.

The simulation shown that the FL Controller is superior when compared to PI controllers and fixed current compensation. By using an FLC, nominal voltage is achieved in the shortest amount of time, with the smallest voltage drops, and the most efficient use of energy. In this study, the FLC restored nominal voltage during MVIM-1 startup in 4.97 seconds, the PI controller took 5.09 seconds, the fixed controller took 5.46 seconds, and without compensation took 6.96 seconds. The energy stored in the SC used to compensate for the inrush current of MVIM-1 was calculated from the voltage difference in SC. The initial voltage minus the end voltage of the SC shown in Table 2 controlled by FLC is 92 volts. This value is equal to 5.92 kWH.

Simulations with lump loads and a series of induction motors starting showed the efficiency in electrical power consumption. Starting the MVIM showed a 36.84 % power consumption efficiency. This ensures a smoother and more reliable induction motor starting process. These findings highlight the potential of the multifunction PV farm for optimizing electrical power consumption in industrial settings, while also addressing the challenges associated with inrush current when an MVIM is being started.

Notation

52	ANSI for AC Circuit Breaker
C	Compensation
CT	Current Transformer
FACTS	Flexible AC Transmission System
FLC	Fuzzy Logic Controller
INV	Inverter
LVRT	Low Voltage Ride Through
MF	Membership Function (Fuzzy)
MFR	Multi-Function Relay
Mtr	Induction Motor
MV	Medium Voltage
MVIM	Medium Voltage Induction Motor
PID	Proportional Integral and Derivative
PT	Power Transformer
PV	Photo Voltaic
SC	Supercapacitor
VS	Voltage Sag
VT	Voltage Transformer
XFMR	Transformer

Acknowledgment

This research was funded by the Ministry of Research, Technology and Higher Education, Indonesia, under the PDD (Penelitian Disertasi Doktor) scheme.

References

[1] Melfi, M. J., & Umans, S. D. (2012). Squirrel-cage induction motors: Understanding starting transients. *IEEE Industry Applications Magazine*, *18*(6), 28–36. https://doi.org/10.1109/MIAS.2012.2210091

[2] Ledoux, K., Visser, P. W., Hulin, J. D., & Nguyen, H. (2015). Starting large synchronous motors in weak power systems. *IEEE Transactions on Industry Applications*, *51*(3), 2676–2682. https://doi.org/10.1109/TIA.2014.2373820

[3] *1668-2017 - IEEE Recommended Practice for Voltage Sag and Short Interruption Ride-Through Testing for End-Use Electrical Equipment Rated Less than 1000 V*. (2017). IEEE.

[4] Ntare, R., Abbasy, N. H., & Youssef, K. H. M. (2019). Low Voltage Ride through Control Capability of a Large Grid Connected PV System Combining DC Chopper and Current Limiting Techniques. *Journal of Power and Energy Engineering*, *07*(01), 62–79. https://doi.org/10.4236/jpee.2019.71004

[5] Nelson, R. (2012). Fault Ride-Through trip curves. *IEEE Power and Energy Society General Meeting*. https://doi.org/10.1109/PESGM.2012.6343983

[6] Menteri Energi dan Sumbar Daya Mineral Republik Indonesia (2020). Peraturan Menteri Energi dan Sumber Daya Mineral Republik Indonesia nomor 20 Tahun 2020 tentang Aturan Jaringan Sistem Tenaga Listrik (Grid Code). https://jdih.esdm.go.id/index.php/web/result/2120/detail.

[7] Aaron, H., Thomas, JN., Thomas, JD., Gianni, P., Kevin, A. (2019). Exploring New and Conventional Starting Methods of Large Medium-Voltage Induction Motors on Limited kVA Sources, IEEE Transactions On Industry Applications, Vol. 55, No. 5, pp. 4474-4482, September/October 2019. https://doi.org/10.1109/IAS.2018.8544648

[8] Yong. H., Allan. T., Flexible AC Transmission System (FACTS), (1999). IET Power and Energy Series, Volume 30", The Institue of Electrical Engineers, London.

[9] Nattapol, H.-U., & Bhumkittipich, K. (2019). Improvement of Low Voltage Ride-through Capability of DFIG-based Wind Turbines under Low Voltage Condition; Improvement of Low Voltage Ride-through Capability of DFIG-based Wind Turbines under Low Voltage Condition. In *2019 7th International Electrical Engineering Congress (iEECON)*.

[10] Ren, K., Zhang, X., Wang, F., Guo, L., Wang, Z., & Wang, L. (2016). Grid fault ride through of a medium-voltage three-level full power wind power converter. *2016 IEEE 8th International Power Electronics and Motion Control Conference, IPEMC-ECCE Asia 2016*, 1509–1514. https://doi.org/10.1109/IPEMC.2016.7512515
[11] Zhang, Z., You, X., Ma, H., Zhao, K., & Zhou, N. (2021). Research on Application of Low Voltage Ride through Technology of Auxiliary Equipment Inverter of Thermal Power Plant in Power Grid. *Proceedings - 2021 6th Asia Conference on Power and Electrical Engineering, ACPEE 2021*, 1446–1450. https://doi.org/10.1109/ACPEE51499.2021.9437040
[12] Wang, L., Bai, F., Yan, R., & Saha, T. K. (2018). Real-Time Coordinated Voltage Control of PV Inverters and Energy Storage for Weak Networks with High PV Penetration. *IEEE Transactions on Power Systems*, *33*(3), 3383–3395. https://doi.org/10.1109/TPWRS.2018.2789897
[13] Liu, Y., & Tian, L. (2017). Research on low voltage ride through technology of grid-connected photovoltaic system. *2016 International Conference on Smart Grid and Clean Energy Technologies, ICSGCE 2016*, 212–216. https://doi.org/10.1109/ICSGCE.2016.7876055
[14] Hasanien, H. M. (2016). An Adaptive Control Strategy for Low Voltage Ride Through Capability Enhancement of Grid-Connected Photovoltaic Power Plants. *IEEE Transactions on Power Systems*, *31*(4), 3230–3237. https://doi.org/10.1109/TPWRS.2015.2466618
[15] Shin, D., Lee, K. J., Lee, J. P., Yoo, D. W., & Kim, H. J. (2015). Implementation of fault ride-through techniques of grid-connected inverter for distributed energy resources with adaptive low-pass notch PLL. *IEEE Transactions on Power Electronics*, *30*(5), 2859–2870. https://doi.org/10.1109/TPEL.2014.2378792
[16] Faanzir, F., Ashari, M., Soedibyo, S., Suwito, S., & Umar, U. (2022). The Design of DC Micro Grid with a Load-Based Battery Discharge Method for Remote Island Electrification Utilizes Marine Currents and Solar Photovoltaic. *Kinetik: Game Technology, Information System, Computer Network, Computing, Electronics, and Control*. https://doi.org/10.22219/kinetik.v7i4.1576
[17] Hussain Panhwar, I., Ahmed, K., Seyedmahmoudian, M., Stojcevski, A., Horan, B., Mekhilef, S., Aslam, A., & Asghar, M. (2020). Mitigating power fluctuations for energy storage in wind energy conversion system using supercapacitors. *IEEE Access*, *8*, 189747–189760. https://doi.org/10.1109/ACCESS.2020.3031446
[18] Somayajula, D., & Crow, M. L. (2014). An ultracapacitor integrated power conditioner for intermittency smoothing and improving power quality of distribution grid. *IEEE Transactions on Sustainable Energy*, *5*(4), 1145–1155. https://doi.org/10.1109/TSTE.2014.2334622
[19] Ammar, M., & Joós, G. (2014). A short-term energy storage system for voltage quality improvement in distributed wind power. *IEEE Transactions on Energy Conversion*, *29*(4), 997–1007. https://doi.org/10.1109/TEC.2014.2360071
[20] Ghazanfari, A., Hamzeh, M., Mokhtari, H., & Karimi, H. (2012). Active power management of multihybrid fuel cell/supercapacitor power conversion system in a medium voltage microgrid. *IEEE Transactions on Smart Grid*, *3*(4), 1903–1910. https://doi.org/10.1109/TSG.2012.2194169
[21] Sun, G., Li, Y., Jin, W., Li, S., & Gao, Y. (2019). A Novel Low Voltage Ride-Through Technique of Three-Phase Grid-Connected Inverters Based on a Nonlinear Phase-Locked Loop. *IEEE Access*, *7*, 66609–66622. https://doi.org/10.1109/ACCESS.2019.2912859
[22] Talha, M., Raihan, S. R. S., Rahim, N. A., Akhtar, M. N., Butt, O. M., & Hussain, M. M. (2022). Multi-Functional PV Inverter With Low Voltage Ride-Through and Constant Power Output. *IEEE Access*, *10*, 29567–29588. https://doi.org/10.1109/ACCESS.2022.3158983
[23] Budiman, F. N., & Ramadhani, M. R. (2018). Total Harmonic Distortion Comparison between Sinusoidal PWM Inverter and Multilevel Inverter in Solar Panel. *Kinetik: Game Technology, Information System, Computer Network, Computing, Electronics, and Control*, 191–202. https://doi.org/10.22219/kinetik.v3i3.617
[24] Han, C., Huang, A. Q., Baran, M. E., Bhattacharya, S., Litzenberger, W., Anderson, L., Johnson, A. L., & Edris, A. A. (2008). STATCOM impact study on the integration of a large wind farm into a weak loop power system. *IEEE Transactions on Energy Conversion*, *23*(1), 226–233. https://doi.org/10.1109/TEC.2006.888031
[25] Hermawan, I. B., Ashari, M., & Riawan, D. C. (2022). PV Farm Ancillary Function for Voltage Sag Mitigation Caused by Inrush Current of an Induction Motor. *International Journal of Intelligent Engineering and Systems*, *15*(6), 325–336. https://doi.org/10.22266/ijies2022.1231.31
[26] Mickey, K. (2016). “Process Control A Practical Approach, Second edition.”, Chichester, West Sussex, United Kingdom: John Wiley &Sons Inc.
[27] Suwito, S., Ashari, M., Rivai, M., & Mustaghfirin, M. A. (2022). Enhancement of Photovoltaic Pressurized Irrigation System Based on Hybrid Kalman Fuzzy. *International Journal of Intelligent Engineering and Systems*, *15*(2), 426–440. https://doi.org/10.22266/ijies2022.0430.39